Organic & Biomolecular Chemistry

Accepted Manuscript

ROYAL SOCIETY OF CHEMISTRY

www.rsc.org/obc

Synthesis, antibacterial activities, and theoretical studies of dicoumarols

Jing Li[1§], Zheng Hou[2§], Guang-hui Chen[2§], Fen Li[2], Ying Zhou[2], Xiao-yan Xue[2], Zhou-peng Li[2], Min Jia[2], Zi-dan Zhang[3], Ming-kai Li[2*], Xiao-xing Luo[2*]

1. School of Chemistry and Chemical Engineering, Xi'an University of Arts and Sciences, Xi'an, China
2. Department of Pharmacology, School of Pharmacy, the Fourth Military Medical University, Xi'an, China
3. Department of Physics, School of Science, Tianjin University, Tianjin, China

[§]These authors contributed equally to this work.

[*]Corresponding author: mingkai@fmmu.edu.cn (Ming-kai Li); xxluo3@fmmu.edu.cn (Xiao-xing Luo)

Abstract

Four dicoumarols (DC, 2-PyDC, 3-PyDC and 4-PyDC) were synthesized and characterized via IR, ^{1}H NMR, HRMS, and single crystal X-ray crystallography. Two classical intramolecular O—H···O hydrogen bonds (HBs) stabilized their structures. The total HB energies in DC, 2-PyDC, 3-PyDC and 4-PyDC were performed with the density functional theory (DFT) [B3LYP/6-31G*] method. The in vitro antibacterial activity of DC, 2-PyDC, 3-PyDC and 4-PyDC against *Staphylococcus aureus* (*S. aureus* ATCC 29213), methicillin-resistant *S. aureus* (MRSA XJ 75302), vancomycin-intermediate *S. aureus* (Mu50 ATCC 700699), and USA 300 (Los Angeles County clone, LAC) was evaluated by observing the minimum inhibitory concentration and time–kill curves. The results showed that among all the compounds, 2-PyDC exhibited the most potent antibacterial activity.

Key Words: Dicoumarol, Single crystal, *Staphylococcus aureus*, Minimum inhibitory concentration

1. Introduction

Staphylococcus aureus (*S. aureus*) is a main pathogen responsible for a number of diseases ranging from skin and soft tissue infections to life-threatening endocarditis in hospitals and community settings. *S. aureus* infections are a leading cause of healthcare-associated infections and associated with in-hospital mortality as high as 15% to 60%, especially in critically ill patients[1–3]. Methicillin-resistant *S. aureus* (MRSA) is the cause of major outbreaks and epidemics in hospitalized patients because of the emergence, spread, and rapid evolution of resistance genes developing among pathogens. As such, the mortality and morbidity rates of patients affected by MRSA are high [4, 5]. A number of schemes recently resulted in a dramatic increase in the total number of *S. aureus* bacteremia cases reported annually, and the proportion of such cases involving MRSA increased from 2% in 1990 to > 40% in the early 2000s [6, 7]. Vancomycin is currently the most effective antibiotic treatment for MRSA. However, the emergence of vancomycin-resistant MRSA and the treatment failure of MRSA infections suggest the urgent necessity of developing new antimicrobials.

Coumarin (2H-chromen-2-one) and its derivatives are widely distributed in nature and exhibit a broad pharmacological profile. Dicoumarols are often discussed because of their special molecular structures [two intramolecular O—H···O hydrogen bonds (HBs)] and diverse biological properties through chemical

modifications (different substituents on the central linker methylene). Many studies have recently associated the function of dicoumarols with several bioactivities, including anticoagulant, insecticidal, antihelminthic, hypnotic, and antifungal activities, phytoalexin production, and HIV protease inhibition[8–11]. Given the considerable importance of the compounds, researchers focused on the synthesis of dicoumarol derivatives.

To identify more active compounds, we prepared a series of dicoumarols, namely, 3,3′-methylenedi(4-hydroxycoumarin) (DC), 3,3′-(2-pyridinomethylene)di(4-hydroxycoumarin) (2-PyDC), 3,3′-(3-pyridinomethylene)di(4-hydroxycoumarin) (3-PyDC), and 3,3′-(4-pyridinomethylene)di(4-hydroxycoumarin) (4-PyDC) (Fig. 1), and then evaluated their antibacterial activities. A possible relationship between such hydrogen-bonded structures and their antibacterial activities was further investigated by theoretical calculations.

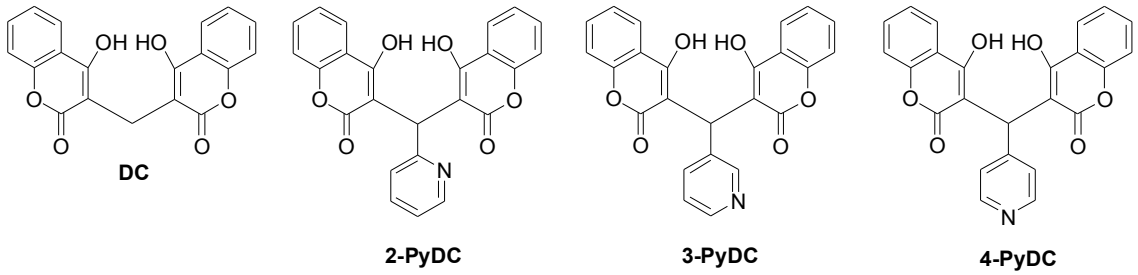

Fig. 1 Chemical structures of DC, 2-PyDC, 3-PyDC and 4-PyDC

2. Results

2.1 Molecular structure

The crystal structure of DC is presented in Fig. 2. In the crystal structure of DC, two 4-hydroxycoumarin moieties are linked through a methylene bridge, on which two classical nearly symmetric intramolecular O—H···O HBs between a hydroxyl group of one coumarin fragment and a lactone carbonyl group of another coumarin fragment further stabilize the entire structure [$d(O_1—O_6)$ = 2.692 Å and $d(O_3—O_4)$ = 2.684 Å].

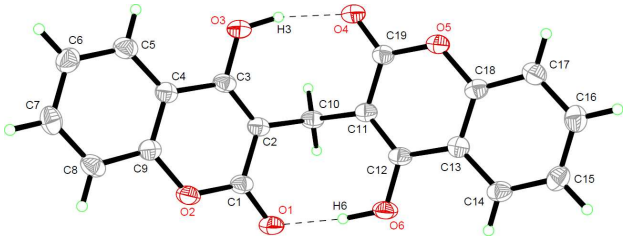

Fig. 2 Crystal structure of compound DC.

2.2 Quantum chemical calculations

2.2.1 Geometric parameters of DC, 2-PyDC, 3-PyDC and 4-PyDC

The fully optimized molecular structures of DC, 2-PyDC, 3-PyDC and 4-PyDC with atomic numbering calculated at B3LYP level of theory [12] are shown in Fig. 3. For compound DC, selected calculated geometric parameters under three different basis sets (6-31G*, 6-31+G**, and 6-311G*) and experimental geometric parameters are presented in Table 1.

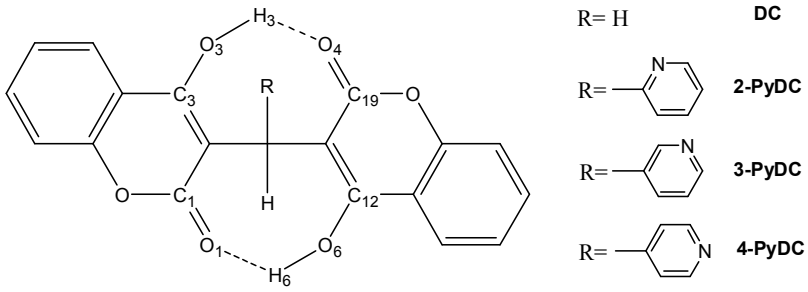

Fig. 3 Schematic presentation of DC, 2-PyDC, 3-PyDC and 4-PyDC

As shown in Table 1, the maximum deviations of the selected bond lengths between theoretical and experimental data were 0.02, 0.018, and 0.019 Å under three different basis sets. The maximum deviations of the selected bond angles between theoretical and experimental data were 0.91°, 1.2°, and 0.95°. The values of the three different basis sets were very close, and the calculated results agreed with the experimental findings. B3LYP/6-31G* exhibited sufficient agreement with experimental data and lower computational cost, so further theoretical study was performed at this level.

Table 1 Experimental and calculated parameters of the selected bond lengths and bond angles of DC

Name definition	DC			
	X-ray	6-31G*	6-31+G**	6-311G*
$R(O_3\cdots O_4)$	2.684	2.697	2.683	2.702
$R(O_1\cdots O_6)$	2.692	2.696	2.683	2.702
$R(C_1{=}O_1)$	1.218	1.233	1.235	1.226
$R(C_1{-}O_2)$	1.355	1.374	1.372	1.373
$R(C_{19}{=}O_4)$	1.224	1.233	1.235	1.226
$R(C_{19}{-}O_5)$	1.354	1.374	1.372	1.373
$R(C_2{-}C_{10})$	1.504	1.513	1.512	1.512
$R(C_{10}{-}C_{11})$	1.501	1.513	1.512	1.512
$A(C_1{-}O_2{-}C_9)$	120.95	121.52	121.56	121.55
$A(O_1{-}C_1{-}O_2)$	116.25	116.23	116.44	116.47
$A(C_{18}{-}O_5{-}C_{19})$	121.41	121.52	121.56	121.55
$A(O_4{-}C_{19}{-}O_5)$	116.44	116.22	116.44	116.47
$A(C_2{-}C_{10}{-}C_{11})$	115.9	115.64	115.77	115.78
$D(C_1{-}C_2{-}C_{10}{-}C_{11})$	90.49	89.58	89.29	89.54
$D(C_{12}{-}C_{11}{-}C_{10}{-}C_2)$	89.49	89.51	89.98	90.09

Table 2 shows the lengths of $O_3\cdots O_4$ and $O_1\cdots O_6$ of 2-PyDC, 3-PyDC, and 4-PyDC under three different basis. The average lengths of $O_3\cdots O_4$ and $O_1\cdots O_6$ for 2-PyDC were 2.621 and 2.716 Å, respectively. For compound 3-PyDC, the corresponding values were 2.629 and 2.699 Å, and for compound 4-PyDC, the corresponding values were 2.632 and 2.696 Å. The length discrepancy between $O_3\cdots O_4$ and $O_1\cdots O_6$ in 2-PyDC, 3-PyDC, and 4-PyDC was greater than that in compound DC. This result is attributed to the structure of compound DC in which two 4-hydroxycoumarin moieties were linked through a

methylene bridge, on which one hydrogen atom was replaced with a pyridine ring forming new structures of 2-PyDC, 3-PyDC, and 4-PyDC.

Table 2 Calculated length of $O_3\cdots O_4$ and $O_1\cdots O_6$ for 2-PyDC, 3-PyDC and 4-PyDC under three different basis.

Compounds	$O_3\cdots O_4$ / Å			$O_1\cdots O_6$ / Å		
	6-31G*	6-31+G**	6-311G*	6-31G*	6-31G*	6-31G*
2-PyDC	2.63810	2.59559	2.62949	2.69648	2.71893	2.73173
3-PyDC	2.63810	2.60811	2.63897	2.69648	2.69107	2.70843
4-PyDC	2.63810	2.61486	2.64391	2.69648	2.68555	2.70508

2.2.2 Estimation of the single and total HB energies in DC, 2-PyDC, 3-PyDC and 4-PyDC

Based on stable PES structures, which were elucidated by structure optimization, single and total HB energies of the four compounds were obtained.

For example, we take compound DC to estimate single and total HB energies. The global minimum structure was stabilized by two hydroxyl bonds (HBs); two higher energy structures were stabilized by one HB (DC1 and DC2).

Table 3 Total electronic energies (in hartree) and HB energies (in kJ/mol) of hydrogen bonded conformers of DC, 2-PyDC, 3-PyDC and 4-PyDC calculated at B3LYP/6-31G* level of theory.

System	Total electronic energies[a]	$E(O_6—H_6\cdots O_1)$	$E(O_3—H_3\cdots O_4)$	E(total HB)
DC	-1182.371051			-119.160943
DC1	-1182.348358	-59.5804715		
DC2	-1182.348358		-59.5804715	
2-PyDC	-1429.370398			-64.939117
2-PyDC1	-1429.361536	-23.267181		
2-PyDC2	-1429.354526		-41.671936	
3-PyDC	-1429.367201			-70.331894
3-PyDC1	-1429.356661	-27.67277		
3-PyDC2	-1429.350953		-42.659124	
4-PyDC	-1429.368219			-68.7697215
4-PyDC1	-1429.357538	-28.0429655		
4-PyDC2	-1429.352707		-40.726756	

[a] ZP corrected.

The $O_6—H_6\cdots O_1$ HB energy was estimated from the energy difference between DC and DC1, $E(O_6—H_6\ldots O_1) = E_{DC}^{coor} - E_{DC1}^{coor}$, calculated to be -59.58 kJ/mol (Table 3). DC1 is a global minimum structure with one HB ($O_3—H_3\cdots O_4$). The $O_3—H_3\cdots O_4$ HB energy was estimated from the energy difference between DC and DC2, $E(O_3—H_3\ldots O_4) = E_{DC}^{coor} - E_{DC2}^{coor}$, calculated to be -59.58 kJ/mol

(Table 3). DC2 was obtained from the global minimum structure of DC, but H_3 was rotated around the C_3—O_3 bond until O_3—H_3···O_4 HB rupture occurred [13, 14]. The total HB energy in DC, calculated by the equation $2E_{DC}^{coor} - (E_{DC1}^{coor} + E_{DC2}^{coor})$, was estimated to be -119.16 kJ/mol (Table 3).

Compared with compound DC, the O_3—H_3···O_4 HB energy for 2-PyDC, 3-PyDC, and 4-PyDC was stronger than O_6—H_6···O_1 HB energy (Table 3) because of the three different pyridine rings introduced in the methylene bridge. The values obtained were consistent with the calculated parameters, that is, the distance of O_3—O_4 was shorter than that of O_6—O_1. The total HB energies for 2-PyDC, 3-PyDC, and 4-PyDC were −64.94, −70.33, and −68.77 kJ·mol^{-1}, respectively (Table 3).

2.2.3 Electron density (ρ_b) and its Laplacian ($\nabla^2\rho_b$) at the bond critical points of DC, 2-PyDC, 3-PyDC and 4-PyDC

The calculated electron density (ρ_b) and its Laplacian ($\nabla^2\rho_b$) at bond critical points for DC, 2-PyDC, 3-PyDC and 4-PyDC are presented in Table 4.

Table 4 shows that the compounds DC, 2-PyDC, 3-PyDC, and 4-PyDC with both HBs exhibited low ρ_b and positive $\nabla^2\rho_b$ values, which further indicated the electrostatic character of the HBs[15].

The HBs in DC were symmetrical, and the calculated ρ_b and $\nabla^2\rho_b$ for the O···H bonding in the upper and lower exocyclic ring was consistent with each other. However, the HBs in 2-PyDC, 3-PyDC, and 4-PyDC were unsymmetrical, and the calculated ρ_b and $\nabla^2\rho_b$ for the O···H bonding in the upper exocyclic ring were higher than those in the lower exocyclic ring. The results were consistent with the stronger HB strength in the upper exocyclic ring for 2-PyDC, 3-PyDC, and 4-PyDC after introducing three different pyridine rings on the methylene group of compound DC (as was found from the calculated HB energies).

Table 4 Properties of the electron density at bond critical points, ρ_b and its Laplacian, $\nabla^2\rho_b$, (a.u.) for DC, 2-PyDC, 3-PyDC and 4-PyDC, calculated at B3LYP/6-31G* level of theory

Bond	DC		2-PyDC		3-PyDC		4-PyDC	
	ρ_b	$\nabla^2\rho_b$	ρ_b	$\nabla^2\rho_b$	ρ_b	$\nabla^2\rho_b$	ρ_b	$\nabla^2\rho_b$
Upper exocyclic ring								
O_3—H_3	0.3059	-1.5668	0.3039	-1.5548	0.3042	-1.5567	0.3044	-1.5567
C_3—O_3(—H_3)	0.3118	-0.3428	0.3157	-0.3371	0.3156	-0.3348	0.3156	-0.3358
C_{19}=O_4	0.3979	-0.1114	0.4003	-0.0752	0.4005	-0.0789	0.4005	-0.0794
O_4···H_3	0.0444	0.1363	0.0485	0.1513	0.0483	0.1520	0.0483	0.1523
Lower exocyclic ring								
O_6—H_6	0.3059	-1.5667	0.3076	-1.5762	0.3071	-1.5768	0.307	-1.5766
C_{12}—O_6(—H_6)	0.3118	-0.3427	0.3103	-0.3464	0.3107	-0.3578	0.3108	-0.3586
C_1=O_1	0.3979	-0.1112	0.3975	-0.1196	0.3974	-0.1177	0.3974	-0.1173
O_1···H_6	0.0444	0.1363	0.0443	0.1379	0.0443	0.1372	0.0444	0.1371

2.3 Minimal inhibitory concentration (MIC) assay

Four *S. aureus* bacterial strains, including one drug-sensitive *S. aureus* (*S. aureus* ATCC 29213) strain and three MRSA strains (MRSA XJ 75302, Mu50, USA 300 LAC), were used in the systematic analysis of the antibacterial activities of DC, 2-PyDC, 3-PyDC and 4-PyDC in vitro. Because of the liposolubility of the four compounds, they were dissolved into the solution with 1% Dimethyl sulfoxide (DMSO) at final

concentration. As shown in Table 5, among the compounds, 2-PyDC exerted the most potent bactericidal effects against nearly all types of *S. aureus* tested, including USA 300 LAC, which is a highly virulent and widespread clinical isolate that causes the recent epidemic of MRSA infections. The MIC values of 2-PyDC ranged from 16 to 64 μg/mL. By contrast, other compounds exerted weaker bactericidal effects against *S. aureus*, and their MIC values exceed 256 μg/mL for *S. aureus* (ATCC 29213) and the three MRSA strains. Compared with the MIC values of the above compounds, the MIC values of levofloxacin, ceftazidime, ceftriaxone, gentamicin and piperacillin against *S. aureus* (ATCC 29213) strains were lower (less than 8 μg/mL) but were higher against resistant strains at varying degrees. The results showed that 2-PyDC has the most potent broad-spectrum antibacterial activity on the drug-sensitive and drug-resistant *S. aureus* in vitro.

Table 5 MIC of DC, 2-PyDC, 3-PyDC, 4-PyDC and antibiotics in Mueller-Hinton Broth Culture.

Drugs	MIC (ug/mL)			
	S. aureas (ATCC 29213)	MRSA (XJ 75302)	Mu50 (ATCC 700699)	LAC (USA 300)
DC	>256	>256	>256	>256
2-PyDC	16	64	32	64
3-PyDC	>256	>256	>256	>256
4-PyDC	>256	>256	>256	>256
Levofloxacin	<0.125 (S)	4 (R)	4 (R)	8 (R)
Ceftazidime	8 (S)	>256 (R)	256 (R)	64 (R)
Ceftriaxone	2 (S)	>256 (R)	256 (R)	32 (R)
Gentamicin	0.12 (S)	64 (R)	32 (R)	0.25 (S)
Piperacillin	2 (S)	>128 (R)	>128 (R)	8 (R)

S means drug susceptibility, *R* means drug resistance. Levofloxacin, ceftazidime, ceftriaxone, gentamicin, and piperacillin as control antibiotics exert anti-bacterial effects on the drug-susceptible *S. aureas* strain (ATCC 29213). MRSA (XJ 75302) and Mu50 (ATCC 700699) are resistant to all of the control antibiotics, whereas LAC (USA 300) is susceptible to gentamicin but resistant to the other control antibiotics. Compared with DC (3-PyDC and 4-PyDC), 2-PyDC has more potent effects on the bacterials listed above.

2.4 Bacterial growth inhibition

We further investigated the growth inhibitory and bactericidal effects to gain insight into the mode of action of compound 2-PyDC. Additional experiments were performed to determine the growth rate of *S. aureus* in liquid medium containing the different concentrations of the compound. The compound 2-PyDC was added to cultures at concentrations of 4, 8, 16, 32 or 64 μg/mL to evaluate the growth inhibitory effects on *S. aureus* ATCC 29213, MRSA XJ 75302, Mu50, and MRSA USA 300 LAC. As shown in Fig. 4A, 2-PyDC significantly inhibited the growth of the drug-sensitive *S. aureus* ATCC 29213 at 16 μg/mL and exhibited almost complete growth inhibition on this pathogen at 32 or 64 μg/mL. Although 2-PyDC was not able to effectively inhibited the growth of the drug-resistant strains MRSA XJ 75302 (Fig. 4B), exhibited almost complete growth inhibition on Mu50 (Fig. 4C), and MRSA USA 300 LAC (Fig. 4D) at 16,

32 or 64 μg/mL. Similar to the results of the MIC values, the other compounds hardly showed any inhibitory effects on these pathogens at these concentrations (data was not shown). *S. aureus* growth in MH broth without any compounds, which was used as the control sample, did not exhibit any significant growth inhibitory effect. The analysis of bacterial growth inhibition showed that aside from exerting antibacterial activities on *S. aureus,* 2-PyDC also inhibited the growth of the drug-sensitive and drug-resistant *S. aureus* strains.

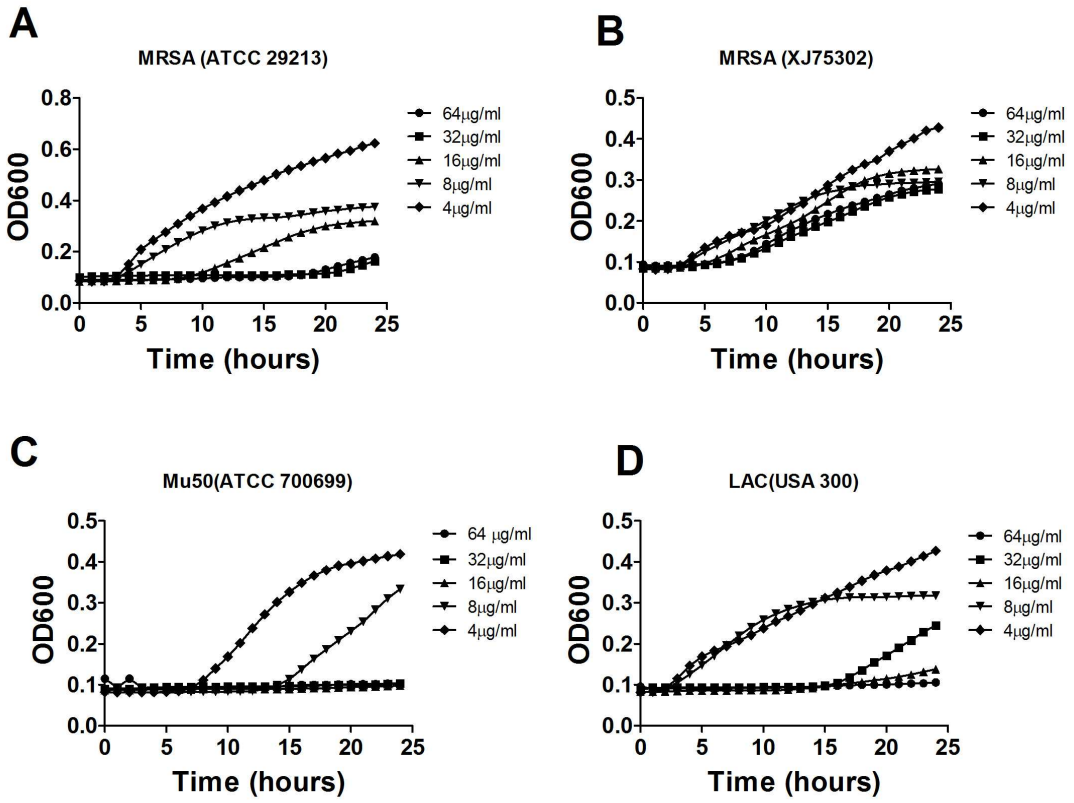

Fig. 4 Concentration-dependent inhibition of compound 2-PyDC on the growth of *S. aureus* ATCC 29213, MRSA XJ 75302, Mu50, and MRSA USA 300 LAC. The cells were cultured in liquid culture medium and treated with different concentrations of compound 2-PyDC.

2.5 In Vitro Toxicity measurement

To further explore the safety for the possible development, we investigated compound 2-PyDC cytotoxicity to human umbilical vein endothelial cells (HUVECs) and human embryonic cardiomyocytes cell line CCC-HHM-2 (HHHM-2) in vitro. As shown in Fig. 5, there was no significant difference on cell viability between the control group and compound 2-PyDC treated group under concentration of 200 μg/mL ($P > 0.05$), and the IC50 to the HUVECs and HHHM-2 was 765.34 μg/mL and 786.96 μg/mL, respectively. These results implied that compound 2-PyDC had much less toxicity to mammalian cells, and had a relatively wide safety range for potential antimicrobial applications.

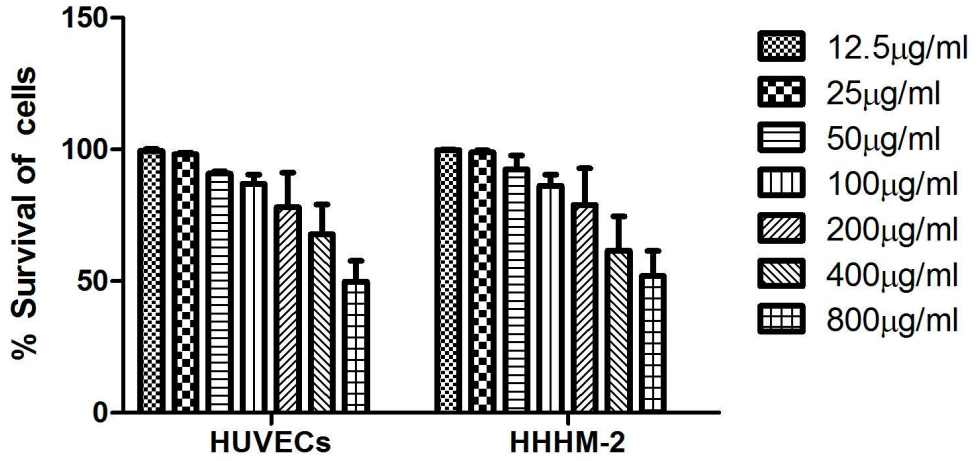

Fig. 5 Cytotoxicity measurement of compound 2-PyDC on the human umbilical vein endothelial cells (HUVECs) and human embryonic cardiomyocytes cell line CCC-HHM-2 (HHHM-2) in vitro. There was no significant difference on cell viability between the control group and compound 2-PyDC treated group under concentration of 200 μg/mL (P> 0.05).

3. Discussion

To get ahead of the problem on resistance, we must look for first-in-class antibacterials and new targets. Anti-bacterial activity and drug resistance of bacteria have a close relationship with the structure of antibiotics, hence the discovery of antibiotics with novel structures and the development of drugs against MRSA are highly active fields [16, 17]. Dicoumarols is a plant-derived natural product known for its wide pharmacological properties, such as anti-inflammatory and anticoagulant attributes [18]. No antibiotic that has a similar structure as dicoumarol derivatives is clinically being used for infection treatment. In this work, novel dicoumarol derivative 2-PyDC was demonstrated to be capable of significantly inhibiting the growth of multi-drug-resistant *S. aureus*. The MIC values showed the efficacy of 2-PyDC at a range of 16 to 64 μg/mL against *S. aureus* (ATCC 29213), MRSA (XJ 75302), Mu50, and USA 300. To confirm the anti-MRSA activity of 2-PyDC, bacterial growth inhibition rate using time-kill curves was evaluated. The concentration-dependent inhibition of 2-PyDC on the growth of *S. aureus* (ATCC 29213), MRSA (XJ 75302), Mu50, and USA 300 was consistent with the MIC results, wherein 32 or 64 μg/mL 2-PyDC significantly inhibited the growth of MRSA. However, compared with 2-PyDC, other three compounds exerted almost no effect on any *S. aureus* in the MIC or growth inhibition rate experiments.

The experiment results also showed that all four compounds consisted of a 4-hydroxycoumarin dimer containing two classical intramolecular O—H···O HBs, which were considered as important factors in assisting the molecule to obtain the correct configuration for biological activity[19]. The calculated results were credible based on the fact that the fully optimized molecular structures of DC calculated at B3LYP level of the theory using three different basis sets (6-31G*, 6-31+G** and 6-311G*) were in agreement with its available X-ray data.

Because of the three different pyridine rings individually introduced in the methylene bridge destroying the symmetrical structure of DC, the calculated ρ_b and $\nabla^2\rho_b$ for the O···H bonding in the upper exocyclic ring were higher than that in the lower exocyclic ring for compounds 2-PyDC, 3-PyDC, 4-PyDC. Based on the same reason, the total HB stabilization energies in 2-PyDC, 3-PyDC, and 4-PyDC were

estimated to be −64.94, −70.33 and −68.77 kJ/mol, respectively, which were lower than that in compound DC. These values suggest that the most potent antibacterial activity in 2-PyDC correlated with its weakest total HB energy in the four compounds.

4. Conclusion

More appropriate antibiotics should be developed to treat infected patients because of the emergence of methicillin-resistant, vancomycin-intermediate resistant, or multi-drug resistant *S. aureus*. Among the the four compounds, 2-PyDC exhibited the most potent anti-bacterial efficiency, possibly because the 2-pyridine group on the methylene group further weakened the HB strengths. The character of much less toxicity to mammalian cells also exhibits the potential antimicrobial applications. To further define the mechanism underlying the anti-bacterial activity of the derivative and evaluate correlations with its drug efficacy in vivo, additional experiments should be carried out.

5. Experimental

5.1 Apparatus and materials

IR spectra (400-4000 cm^{-1}) were obtained using a Brucker Equinox-55 spectrophotometer. ^1H NMR spectra were obtained using a Varian Inova-400 spectrometer (at 400 MHz). Mass spectra were obtained using a micrOTOF-Q II mass spectrometer. The melting points were taken on a XT-4 micro melting apparatus, and the thermometer was uncorrected.

All antibiotics used were purchased from the National Institute for the Control of Pharmaceutical and Biological Products (Beijing, China). All other chemicals and solvents were of analytical grade.

MRSA (XJ 75302) was isolated from cultures of sputum samples from patients in Xijing Hospital (Xi'an, China). *S. aureus* strain (ATCC 29213) was purchased from the Chinese National Center for Surveillance of Antimicrobial Resistance. Mu50 (ATCC 700699) and USA 300 (LAC) were purchased from MicroBiologics (MN, USA).

5.2 Synthesis and characterization of DC, 2-PyDC, 3-PyDC and 4-PyDC

DC, 2-PyDC, 3-PyDC and 4-PyDC were synthesized according to the methods of a previous report [20]. A mixture of formaldehyde (or pyridine-2-carbaldehyde, pyridine-3-carbaldehyde and pyridine-4-carbaldehyde) (10 mmol) and 4-hydroxycoumarin (20 mmol) was dissolved in 100 mL of EtOH. A few drops of piperidine were added, and the mixture was stirred for 3 h at room temperature. After reaction completion as determined by TLC, water was added until precipitation occurred. After filtering the precipitates, they were sequentially washed with ice-cooled water and ethanol and then dried in a vacuum.

3,3′-Methylenedi(4-hydroxycoumarin) (dicoumarol, DC): Yield: 65%. m.p. 289–290 °C. IR(KBr pellet cm^{-1}): 3051(OH), 1645(CO), 1526(C=C). ^1H NMR ($CDCl_3$, δ, ppm): 11.322(s, 2H), 7.988-8.011(q, 2H), 7.571-7.614(m, 2H), 7.347-7.393(m, 4H), 3.847(s, 2H). HRMS (ESI^+): *m*/*z*: calcd for $C_{19}H_{12}O_6$: 359.0526 [$M+Na^+$]; found: 359.0544.

3,3′-(2-Pyridinomethylene)di(4-hydroxycoumarin) (2-PyDC): Yield: 70%. m.p. 264–265 °C. IR(KBr pellet cm^{-1}): 3053(OH), 1668(CO), 1550(C=C). ^1H NMR (DMSO-d_6, δ, ppm): 8.623-8.637(d, 1H), 8.435-8.474(t, 1H), 7.805-7.909(m, 4H), 7.559-7.598(t, 2H), 7.253-7.348(m, 4H), 6.518(s, 1H). HRMS (ESI^+): *m*/*z*: calcd for $C_{24}H_{15}NO_6$: 436.0792 [$M+Na^+$]; found: 436.0722.

3,3′-(3-Pyridinomethylene)di(4-hydroxycoumarin) (3-PyDC): Yield: 60%. m.p. 280–281 °C. IR(KBr pellet cm^{-1}): 3060(OH), 1665(CO), 1556(C=C). ^1H NMR (DMSO-d_6, δ, ppm): 8.644-8.709(t, 2H), 8.334-8.354(d, 1H), 7.902-7.936(q, 1H), 7.801-7.821(t, 2H), 7.531-7.573(m, 2H), 7.238-7.319(m, 4H), 6.411(s, 1H). HRMS (ESI^+): *m*/*z*: calcd for $C_{24}H_{15}NO_6$: 436.0792 [$M+Na^+$]; found: 436.0689.

3,3′-(4-Pyridinomethylene)di(4-hydroxycoumarin) (4-PyDC): Yield: 70%. m.p. 278–279 °C. IR(KBr

pellet cm^{-1}): 3048(OH), 1662(CO), 1551(C=C). ^1H NMR (DMSO-d_6, δ, ppm): 8.659-8.675(d, 2H), 7.803-7.823(q, 4H), 7.540-7.582(m, 2H), 7.246-7.331(m, 4H), 6.452(s, 1H). HRMS (ESI^+): *m*/*z*: calcd for $C_{24}H_{15}NO_6$: 436.0792 [$M+Na^+$]; found: 436.0786.

5.3 X-ray crystallography

For X-ray diffraction experiments, single crystals of compound DC were both grown from methanol. The X-ray diffraction data were collected on a Bruker SMART APEX II CCD diffractometer equipped with a graphite monochromated Mo Kα radiation (λ = 0.71073 Å) by using the ω-2θ scan technique at room temperature. The structure was solved by direct methods using SHELXS-97 [21] and refined using the full-matrix least squares method on F^2 with anisotropic thermal parameters for all non-hydrogen atoms by using SHELXL-97. Hydrogen atoms were generated geometrically. The crystal data and details concerning data collection and structure refinement are given in Table 6. Molecular illustrations were prepared using the XP package. Parameters in CIF format are available as Electronic Supplementary Publication from Cambridge Crystallographic Data Centre.

Table 6 Crystal data, data collection and structure refinement of compound DC

Formula	$C_{19}H_{12}O_6$
*M*r	336.06
Temperature / K	293
Crystal system	Monoclinic
Space group	$P2_1/c$
a / Å	8.403(6)
b / Å	15.083(10)
c / Å	11.686(8)
α / °	90
β / °	98.565(6)
γ / °	90
V / $Å^3$	1464.6(17)
Z	4
D_{calc} / $g \cdot cm^{-3}$	1.525
μ(Mo Kα) / mm^{-1}	0.115
θ range / °	3.11 to 24.99
Reflections collected	7660
No. unique data[*R*(int)]	2550[0.0182]
No. data with $I \geq 2\sigma(I)$	2204
R_1	0.0447
ωR_2(all data)	0.1270
CCDC	989415

5.4 Quantum chemical calculations

All calculations were carried out using the Gaussian 09 package [22]. Density functional theory (DFT) [23, 24], Becke's three-parameter hybrid function (B3LYP) [25], and LYP correlation function [26, 27] were used to fully optimize all the geometries on the energy surface without constraints. To obtain precise results that are in conjunction with experimental results, three basis sets, namely 6-31G*, 6-31+G**, and 6-311G*, were tested. Frequency calculations at the B3LYP (with basis sets 6-31G*) level of theory were carried out to confirm stationary points as minima and to obtain the zero-point energies and the thermal correlation

data at 1 atm and 298 K.

5.5 Minimal inhibitory concentration (MIC) assay

Based on the CLSI broth microdilution method [28], the determination of minimum inhibitory concentrations (MICs) via microdilution assay was performed in sterilized 96-well polypropylene microtiter plates (Sigma–Aldrich) in a final volume of 200 μL. Bacteria were grown overnight in nutrient broth. Mueller–Hinton (MH) broth (100 μL) containing bacteria (5×10^5 CFU/mL) was added to 100 μL of the culture medium containing the test compound (0.12 μg/mL to 256 μg/mL in serial twofold dilutions). The plates were incubated at 37 °C for 20 h in an incubator. About 50 μL of 0.2% triphenyl tetrazolium chloride (TTC), a colorimetric indicator, was added to each well of microtiter plates and incubated at 35 °C for 1.5 h. The TTC-based MIC was determined as the lowest concentration of oxacillin that showed no red color change indicating complete growth inhibition.

5.6 Bacterial growth inhibition

To obtain the time–kill curves for methicillin-susceptible *S. aureus* and MRSA, the synthetic compounds and antibiotics were added to strain cultures to a final concentration of 4, 8, 16, 32 or 64 μg/mL [29]. The strains were cultivated in the automated Bioscreen C system (Lab systems Helsinki, Finland) by using an MH broth culture medium. The working volume in the wells of the Bioscreen plate was 300 μL, which comprised 150 μL of the MH broth and 150 μL of the drug solution. The temperature was controlled at 35°C, and the optical density of the cell suspensions was measured automatically at 600 nm in regular intervals of 10 min for 20 h. Before each measurement, the culture wells were automatically shaken for 60 s. Statistical data for each experiment were obtained from at least two independent assays performed in duplicate.

5.7 Cytotoxicity assay

The cytotoxicity of compounds to the human umbilical vein endothelial cells (HUVECs) and human embryonic cardiomyocytes cell line CCC-HHM-2 (HHHM-2) was determined by 3-(4,5-dimethyl-2-thiazolyl)-2,5-diphenyl-2-H-tetrazolium bromide (MTT) staining. Briefly, cells (5×10^3 cells/well) were seeded in a 96-well plate with 100 μL DMEM media with 20% fetal bovine serum (FBS) in every well for 12 hours, and then treated with or without compounds at various concentrations (12.5-800 μg/mL) for 24 hours. After treatment, MTT solution (final concentration, 0.5%) was added and cells were incubated for another 4 hours at 37°C. 150 μL DMSO was added to each well after removal of the supernatant and the absorbance at 490 nm was measured with a microplate reader.

Acknowledgments

This work was supported by grants from the National Natural Science Foundation of China (No. 81001460 and No. 81273555) and the Innovation plan of science and technology of Shaanxi Province (2014KTCL03-03).

The authors thank the High Performance Computing Center of Tianjin University and Prof. Xue-hao He for the services provided.

Notes and References

1. P. G. Frisina, A. M. Ann M. Kutlik and A. M. Barrett, *Arch. Phys. Med. Rehab.*, 2013, **94**, 516.
2. M. W. Climo, D. S. Yokoe, D. K. Warren, T. M. Perl, M. Bolon, L. A. Herwaldt, R. A. Weinstein, K. A. Sepkowitz, J. A. Jernigan, K. Sanogo and E. S. Wong, *N. Engl. J. Med.*, 2013, **368**, 533.
3. M. E. Kutcher, A. R. Ferguson and M. J. Cohen, *J. Trauma Acute Care Surg.*, 2013, **74**, 1223.
4. A. K. Seth, M. R. Geringer, K. T. Nguyen, S. P. Agnew, Z. Dumanian, R. D. Galiano, K. P. Leung, T. A. Mustoe and S. J. Hong, *Plast. Reconstr. Surg.*, 2013, **131**, 225.

5. R. Kouyos, E. Klein and B. Grenfell, *PLoS Pathog.*, 2013, **9**, e1003134.
6. D. H. Bor, S. Woolhandler, R. Nardin, J. Brusch and D. U. Himmelstein. *PLoS One*, 2013, **8**, e60033.
7. M. Z. David, S. Medvedev, S. F. Hohmann, B. Ewigman and R. S. Daum, *Infect. Control Hosp. Epidemiol.*, 2012, **33**, 782.
8. B. S. Kirkiacharian, E. D. Clercq, R. Kurkjian and C. Pannecouque, *Pharm. Chem. J.*, 2008, **42**, 265.
9. C. A. Kontogiorgis and D. J. Hadjipavlou-Litina, *J. Med. Chem.*, 2005, **48**, 6400.
10. I. Manolov, C. Maichle-Moessmer and N. Danchev, *Eur. J. Med. Chem.*, 2006, **41**, 882.
11. T. Ojala, S. Remes, P. Haansuu, H. Vuorela, R. Hiltunen, K. Haahtela and P. Vuorela, *J. Ethnopharmacol.*, 2000, **73**, 299.
12. C. Wang, R. Zhang and Z. Lin, *J. Theor. Comput. Chem.*, 2012, **11**, 1237.
13. N. Trendafilova, G. Bauer and T. Mihaylov, *Chem. Phys.*, 2004, **302**, 95.
14. T. Mihaylov, I. Georgieva, G. Bauer, I. Kostova, I. Manolov and N. Trendafilova, *Int. J. Quantum Chem.*, 2006, **106**, 1304.
15. R. F. W. Bader, P. J. MacDougall and C. D. H. Lau, *J. Am. Chem. Soc.*, 1984, **106**, 1594.
16. C. I. Kang and J. H. Song, *Infect. Chemother.*, 2013, **45**, 22.
17. M. Bassetti, M. Merelli, C. Temperoni and A. Astilean, *Ann. Clin. Microbiol. Antimicrob.*, 2013, **12**, 22.
18. F. Borges, F. Roleira, N. Milhazes, L. Santana and E. Uriarte, *Curr. Med. Chem.*, 2005, **12**, 887.
19. B. Schiøtt, B. B. Iversen, G. K. H. Madsen and T. C. Bruice, *J. Am. Chem. Soc.*, 1998, **120**, 12117.
20. N. Hamdi, M. C. Puerta and P. Valerga, *Eur. J. Med. Chem.*, 2008, **43**, 2541.
21. G. M. Sheldrick, SHELXL-97, *Program for Solution Crystal Structure and Refinement*, University of Göttingen, Germany, 1997.
22. M. J. Frisch, G. W. Trucks, H. B. Schlegel, G. E. Scuseria, M. A. Robb, J. R. Cheeseman, G. Scalmani, V. Barone, B. Mennucci, G. A. Petersson, H. Nakatsuji, M. Caricato, X. Li, H. P. Hratchian, A. F. Izmaylov, J. Bloino, G. Zheng, J. L. Sonnenberg, M. Hada, M. Ehara, K. Toyota, R. Fukuda, J. Hasegawa, M. Ishida, T. Nakajima, Y. Honda, O. Kitao, H. Nakai, T. Vreven, J. A. Montgomery, Jr., J. E. Peralta, F. Ogliaro, M. Bearpark, J. J. Heyd, E. Brothers, K. N. Kudin, V. N. Staroverov, R. Kobayashi, J. Normand, K. Raghavachari, A. Rendell, J. C. Burant, S. S. Iyengar, J. Tomasi, M. Cossi, N. Rega, J. M. Millam, M. Klene, J. E. Knox, J. B. Cross, V. Bakken, C. Adamo, J. Jaramillo, R. Gomperts, R. E. Stratmann, O. Yazyev, A. J. Austin, R. Cammi, C. Pomelli, J. W. Ochterski, R. L. Martin, K. Morokuma, V. G. Zakrzewski, G. A. Voth, P. Salvador, J. J. Dannenberg, S. Dapprich, A. D. Daniels, O. Farkas, J. B. Foresman, J. V. Ortiz, J. Cioslowski, and D.J. Fox, Gaussian, Inc., Wallingford CT, Gaussian 09, Revision A.02, 2009.
23. P. Hohenberg and W. Kohn, *Phys. Rev.*, 1964, **136**, B864.
24. W. Kohn and L. J. Sham, *Phys. Rev.*, **1965**, 140, A1133.
25. A. D. Becke, *J. Chem. Phys.*, 1993, **98**, 5648.
26. C. Lee, W. Yang and R. G. Parr. *Phys. Rev. B*, 1988, **37**, 785.
27. B. Miehlich, A. Savin, H. Stoll and H. Preuss, *Chem. Phys. Lett.*, 1989, **157**, 200.
28. Clinical and Laboratory Standards Institute, *Performance Standards for Antimicrobial Susceptibility Testing: Nineteenth Informational Supplement M100-S19*, Wayne, PA, USA, 2009.
29. M. Motyl, K. Dorso and J. Barrett, *Current Protocols in Pharmacology*, New York, 2005, 13A.3.1-22.

figure legends：

Fig. 1 Chemical structures of DC, 2-PyDC, 3-PyDC and 4-PyDC

Fig. 2 Crystal structure of compound DC.

Fig. 3 Schematic presentation of DC, 2-PyDC, 3-PyDC and 4-PyDC.

Fig. 4 Concentration-dependent inhibition of compound 2-PyDC on the growth of *S. aureus* ATCC 29213, MRSA XJ 75302, Mu50, and MRSA USA 300 LAC. The cells were cultured in liquid culture medium and treated with different concentrations of compound 2-PyDC.

Fig. 5 Cytotoxicity measurement of compound 2-PyDC.

Table 1 Experimental and calculated parameters of the selected bond lengths and bond angles of DC

Table 2 Calculated length of $O_3\cdots O_4$ and $O_1\cdots O_6$ for 2-PyDC, 3-PyDC and 4-PyDC under three different basis.

Table 3 Total electronic energies (in hartree) and HB energies (in kJ/mol) of hydrogen bonded conformers of DC, 2-PyDC, 3-PyDC and 4-PyDC calculated at B3LYP/6-31G* level of theory.

Table 4 Properties of the electron density at bond critical points, ρ_b and its Laplacian, $\nabla^2\rho_b$, (a.u.) for DC, 2-PyDC, 3-PyDC and 4-PyDC, calculated at B3LYP/6-31G* level of theory

Table 5 MIC of DC, 2-PyDC, 3-PyDC, 4-PyDC and antibiotics in Mueller-Hinton Broth Culture.

Table 6 Crystal data, data collection and structure refinement of compound DC